Dielectric breakdown in continuous models of metal-loaded dielectrics

Mark F. Gyure* and Paul D. Beale
Department of Physics, University of Colorado, Boulder, Colorado 80309
and Electromagnetic Applications, P.O. Box 26263, Denver, Colorado 80226-0263
(Received 4 November 1991; revised manuscript received 7 May 1992)

We develop two- and three-dimensional models for breakdown of metal-loaded dielectrics based on the breakdown of random arrays of perfectly conducting cylinders and spheres embedded in a uniform dielectric and placed in a uniform external electric field. We determine the breakdown field, breakdown-path geometry, and dielectric constant as a function of metal packing fraction. The computer solution of Laplace's equation in the random geometry uses truncated multipole expansions and the random packing configurations are generated by the Monte Carlo method. We compare the simulation results with exact lower bounds for the dielectric constant and scaling arguments for the breakdown field, which predict a linear relationship between the breakdown field and both the average surface-to-surface spacing between the metal particles and the minimum dielectric gap. Finally, we show that experimental results for inert rocket propellents are in excellent agreement with the scaling prediction.

I. INTRODUCTION

This paper addresses the problem of dielectric breakdown in metal-loaded dielectrics, which are materials consisting of an inhomogeneous mixture of conducting and insulating components. One example is solid fuel rocket propellant, which consists of a mixture of aluminum and ammonium perchlorate particles in a polymer binder. It has been observed[1] that the breakdown field of this materials is lowered significantly by the presence of the aluminum particles and is a strong function of the volume fraction of these particles. This unusually large sensitivity to breakdown is a safety concern in the handling and processing of solid rocket propellants and has been implicated in several accidents involving the ignition of these propellants under conditions where static electric fields are believed to have been present.[1] Our objective is to understand factors relating to breakdown phenomena in these types of materials and to make comparisons with some experimental results on the dielectric breakdown of inert solid rocket propellants.

In this paper we describe two models for dielectric breakdown of these materials based on the solution of Laplace's equation in a medium consisting of random arrays of conducting cylinders [a two-dimensional (2D) model] and spheres [a three-dimensional (3D) model] embedded in a uniform dielectric and placed in a uniform external field. In Sec. II, we begin by describing the construction of randomly inhomogeneous systems of the type mentioned above and outlining the procedure for the solution of the Laplace equation for such systems. We then discuss the breakdown dynamics for this model by defining local breakdowns, global breakdown and the breakdown field. Finally in Sec. II, we define the effective dielectric constant for these systems. In Sec. III, we present some results of this model and make comparisons to previous work on the breakdown of metal-loaded dielectrics. In particular, we study the dependence of the breakdown field E_b on the area and volume fraction of conducting particles. We also examine the effective dielectric constant ϵ as a function of metal fraction for the randomly inhomogeneous systems and compare it to some analytically derived lower bounds. Finally, we identify two geometrical quantities that scale linearly with E_b over a large range of area and volume fractions. These allow the straightforward determination of the effects of mixture composition in real materials. Section V takes this one step further and outlines a procedure for calculating the average nearest-neighbor particle separation distance, one of the parameters that scales with the breakdown field. The materials are assumed to consist of hard spherical particles of two different sizes randomly distributed in a background dielectric. Experimental results for breakdown of some inert solid rocket propellant samples are compared with our scaling prediction. The average nearest-neighbor aluminum particle separation distance is determined for the propellant samples, and the scaling of the experimentally measured breakdown field with the interparticle spacing is confirmed. Section VI contains a brief summary of our results and a few concluding remarks.

Breakdown phenomena in metal-loaded dielectrics have received some attention in recent years from the standpoint of percolation theory. Theoretical efforts have concentrated on lattice models in an attempt to see if the basic physical mechanisms of breakdown in these materials can be identified. Some efforts have focused on the breakdown of fuse networks,[2,3] while others have concentrated on dielectric breakdown in networks.[4–7] We will briefly review a few of those models that are particularly relevant to our work. One such model is a bond percolation model in which conductors are placed on the bonds of a lattice with probability p and capacitors with probability $(1-p)$. The capacitors are capable of sustaining a 1-V drop, after which they irreversibly fail and become conductors. A voltage is applied across the network, and the capacitor sustaining the largest voltage drop greater than one is failed. The voltage is slowly in-

creased and capacitors are allowed to fail in the manner described above until a conducting path forms across the system. The breakdown field is defined as the ratio of the minimum external voltage required to cause complete failure of the network to the linear dimension of the lattice. One significant result of this model is that the breakdown field $E_b \to 0$ as $p \to p_c$, where p_c is the bond percolation threshold.[4] In addition, E_b scales with ξ^{-1} near p_c, where ξ is the percolation correlation length and therefore E_b scales like $(p_c - p)^{\nu}$.[4] Finally, E_b is smaller for larger lattices and scales with $1/\ln(L)$, where L is the linear system size. In addition to the breakdown field, Bowman and Stroud[5] calculated a parameter $l(p)$, which is proportional to the number of bonds that need to be broken in order to form a conducting path across the system. They showed that this parameter $l(p)$ approaches zero as p approaches p_c, but they did not address whether their parameter l actually corresponds to the minimum number of bonds that need to be broken in order to form a top-to-bottom connection across the lattice, a length usually referred to as the minimum gap.[8] One result of these works is that E_b is a linear function of the minimum gap.

In more recent work[9] we developed a two-dimensional continuum model based on the dielectric breakdown of random arrays of conducting cylinders in a capacitor plate geometry. We showed that the breakdown field scales linearly with the average nearest-neighbor separation distance $\bar{d}$. The breakdown field also scales linearly with the average normalized minimum gap $\bar{x}$ (defined as the length of the path through the system which passes through the minimum amount of dielectric in traversing the system from top to bottom divided by the top-to-bottom distance). Our objective in this work is to further extend this continuum model to larger 2D systems and to 3D systems of spheres randomly distributed in a perfect, lossless dielectric. This composite is placed in a uniform external electric field in order to model the dielectric breakdown behavior. The issue to be addressed in this work is whether or not this alternative uniform field model gives the same kind of scaling behavior as the aforementioned capacitor plate model for substantially larger system sizes in two dimensions, and whether or not three-dimensional systems of random spheres obey similar scaling relationships.

II. MODEL

As a starting point for a uniform field continuum model, we approximate arbitrarily shaped metallic inclusions as perfectly conducting cylinders in two dimensions and perfectly conducting spheres in three dimensions of radius a surrounded by oxide layers $0.01a$ in thickness. The oxide layer is supposed in order to compare our results with breakdown measurements on inert rocket propellant. We will assume that the dielectric properties of the oxide are the same as those of the background dielectric so that the effect of the oxide layers in this model is primarily to prevent any pair of particles from initially making electrical contact. We will still assume that the background dielectric is lossless (zero conductivity) with dielectric constant unity for any applied field up to its breakdown strength. We choose a circular boundary for each sample in two dimensions and a spherical boundary in three dimensions. The particles are placed within the boundary randomly via the Monte Carlo method, subject to the constraints that no two particles, including their oxide layers, overlap, and no surface comes within an oxide layer of the sample boundary.

We apply a uniform external electric field to the samples, in contrast to the capacitor plates used in the random cylinder model;[9] the value of the applied field is set to unity. The reason for using a uniform applied field rather than capacitor plates is that the capacitor plates add a large number of unknowns to the system of equations that must eventually be solved just to maintain a constant potential line in two dimensions. This quickly limits the size of the systems that can be attempted with this kind of model. The problem is more acute in three dimensions because a constant potential surface must be maintained, and this results in an even larger system of equations. This is why 3D systems of spheres were not attempted in the previous work.[9] The capacitor plate method of applying a voltage did have the advantage of providing two surfaces that define in a natural way the point at which the sample has broken down completely, i.e., a top-to-bottom connections. The uniform field approach will make it more difficult to define the condition of global breakdown and the breakdown field for a sample, but it does have one immediate advantage when coupled with the cylindrical and spherical sample geometries. It will be straightforward to define the effective dielectric constant for each sample because analytical solutions exist that relate the polarization of each sample to the dielectric constant. Previously, a cumbersome numerical approach was required.[9] The other advantages of the uniform field approach will soon become clear.

We now turn to the matter of finding the electrostatic potential throughout a given sample that will be used to identify regions of large electric field. It is convenient to write the electrostatic potential as a sum of multiple expansions centered at each particle.[10]

In two dimensions, the expansion is

$$V(\mathbf{r}) = \sum_{j=1}^{N_c} \left[C(j) \ln\left[\frac{a_j}{r_j}\right] + \sum_{n\,(\neq 0)} A(j,n) e^{in\theta_j} \left[\frac{a_j}{r_j}\right]^n \right] + V_{\text{ext}}(\mathbf{r}) , \quad (1)$$

where $V(\mathbf{r})$ is the electrostatic potential at an arbitrary field point $\mathbf{r}$ outside all of the cylinders, $V_{\text{ext}}(\mathbf{r})$ is the potential at point $\mathbf{r}$ due to the externally applied electric field, N_c is the number of cylinders, r_j is the distance from the center of jth cylinder to the field point $\mathbf{r}$, and a_j is the radius of the jth cylinder. The coefficient $C(j)$ is the charge on the jth cylinder and $A(j,n)$ is the nth multipole coefficient for the jth cylinder. In three dimensions, the expansion is in terms of spherical harmonics. It can be written as

$$V(\mathbf{r}) = \sum_{j=1}^{N_s} \sum_{l,m} A(j,l,m) \left[\frac{a_j}{r_j}\right]^{l+1} Y_{l,m}(\theta_j,\phi_j) + V_{\text{ext}}(\mathbf{r}) , \quad (2)$$

where again $V(\mathbf{r})$ is the electrostatic potential at an arbitrary field point $\mathbf{r}$ outside all of the spheres, $V_{\text{ext}}(\mathbf{r})$ is the potential at point $\mathbf{r}$ due to the externally applied electric field, N_s is the number of spheres, r_j is the distance from the center of jth sphere to the field point, and a_j is the radius of the jth sphere. The angles θ_j and ϕ_j are the polar and azimuthal angles from the center of the jth sphere to the field point and the $Y_{l,m}$'s are the spherical harmonics. The $A(j,l,m)$'s are the multipole coefficients and the indices run over $l=0,1,\ldots,\infty$ and $m=-l,-l+1,\ldots,l$. The external potential is due to a uniform electric field oriented along the z axis. In polar coordinates about sphere i this becomes

$$\begin{aligned} V_{\text{ext}}(\mathbf{r}) &= -E_0 Z_i - E_0 r_i \cos(\theta_i) \\ &= -E_0 Z_i - \sqrt{4\pi/3} E_0 r_i Y_{l,0}(\theta_i,\phi_i) , \end{aligned} \tag{3}$$

where Z_i is the z component of the position of the ith sphere. If these series are truncated at $l=l_{\max}$, it is possible to obtain an approximate solution for the electrostatic potential at any point $\mathbf{r}$ in the system. The problem is generating a set of equations for the multipole coefficients that can be solved efficiently. The method we use exploits the properties of orthogonality of cylindrical and spherical harmonics in the following way. We use the fact that the voltage on the surface of a conducting sphere is constant over the surface and takes the value V_i on sphere i:

$$\lim_{|\mathbf{r}-\mathbf{R}_i|\to a} V(\mathbf{r}) = V_i . \tag{4}$$

Multiplying both sides of Eq. (2) by $Y^*_{p,q}(\theta_i,\phi_i)$ and integrating over the surface of sphere i we get

$$\begin{aligned} &\sqrt{4\pi}(V_i + E_0 Z_i)\delta_{p,0}\delta_{q,0} + \sqrt{4\pi/3} E_0 \delta_{p,1}\delta_{q,0} \\ &\quad = A(i,p,q) \\ &\qquad + \sum_{j\,(\neq i),l,m} A(j,l,m) \int d\Omega_i Y^*_{p,q}(\theta_i,\phi_i) \\ &\qquad\qquad \times Y_{l,m}(\theta_j,\phi_j) \left[\frac{a}{r_j}\right]^{l+1} , \end{aligned} \tag{5}$$

where $d\Omega_i$ denotes an integral over the unit sphere centered at the location of sphere i. A similar expression in two dimensions follows from Eq. (1).

Orthogonality can no longer be used in the sum straightforwardly because the harmonics are centered at different points. However, these integrals can be evaluated analytically through the use of so-called off-centered expansions, which express a harmonic centered at the jth particle in terms of harmonics centered at the ith particle times other harmonics expressed in terms of the distances and angles between the particle centers. Such expansions have been developed extensively over the past 100 years by mathematical physicists and others[11–17] as the need for them has arisen with respect to problems of physical interest. Consider two cylinders or spheres separated by vector $\mathbf{R}$. Let the vector from one sphere to a field point be $\mathbf{r}$ and a vector from the center of the other sphere to the field point be $\mathbf{r}'$. The vectors are related by $\mathbf{r}=\mathbf{r}'+\mathbf{R}$. Let $r=|\mathbf{r}|$, $r'=|\mathbf{r}'|$, and $R=|\mathbf{R}|$, where $R>r'$, and let θ be the angle $\mathbf{r}$ makes with the x axis; θ' and Θ are the equivalent angles for $\mathbf{r}'$ and $\mathbf{R}$. The relationship between the multipole expansions about different cylinders is given by

$$\ln(r) = \ln(R) - \sum_{m=1}^{\infty} \frac{(-1)^m}{m} \left[\frac{r'}{R}\right]^m \cos[m(\Theta-\theta')] , \tag{6}$$

and

$$\frac{e^{in\theta}}{r^n} = \frac{e^{in\Theta}}{R^n} \sum_{m=0}^{\infty} \frac{(-1)^m (n+m-1)!}{m!(n-1)!} \left[\frac{r'}{R}\right]^m e^{im(\Theta-\theta')} . \tag{7}$$

These equations are derived by taking the leading term in the limit $k\to 0$ in the identity

$$\begin{aligned} e^{in\theta} N_n(kr) = e^{in\Theta} &\sum_{m=-\infty}^{\infty} (-1)^m J_m(kr') N_{n+m}(kR) \\ &\times e^{im(\Theta-\theta')} , \end{aligned} \tag{8}$$

which is easily derived from equation 8.53.2 in Ref. 18. The functions $J_m(x)$ are the Bessel functions of the first kind, and $N_n(x)$ are the Bessel functions of the second kind. For the three-dimensional formula, the paper by Danos and Maximon[11] is a good reference, their Eq. (34) reads

$$\begin{aligned} \eta_l(kr) Y_{l,m}(\theta,\phi) = \sum_{L,M,\lambda,\mu} &C(l,m,L,M,\lambda,\mu) \\ &\times Y_{L,M}(\Theta,\Phi) Y_{\lambda,\mu}(\theta',\phi') \\ &\times \eta_L(kR) j_\lambda(kr') , \end{aligned} \tag{9}$$

where r, R, r', θ, Θ, and θ' are as before and ϕ, Φ, and ϕ' denote the azimuthal angles, j_l is a spherical Bessel function of the first kind, η_l is a spherical Bessel function of the second kind, $Y_{l,m}$ is a spherical harmonic, and the sum runs over $L,\lambda=0,1,\ldots,\infty, M=-L, -L+1,\ldots,L$ and $\mu=-\lambda,-\lambda+1,\ldots,\lambda$. By taking the leading term in the limit $k\to 0$ we get the following relation:

$$\begin{aligned} \frac{1}{r^{l+1}} Y_{l,m}(\theta,\phi) = \frac{1}{R^{l+1}} &\sum_{\lambda,\mu} D(l,m,\lambda,\mu) Y_{l+\lambda,m-\mu}(\Theta,\Phi) \\ &\times Y_{\lambda,\mu}(\theta',\phi') \left[\frac{r'}{R}\right]^\lambda . \end{aligned} \tag{10}$$

The coefficient $D(l,m,\lambda,\mu)$ involves products of $3j$ symbols[19] and has the value

$$\begin{aligned} D(l,m,\lambda,\mu) = (-1)^{m+\lambda+\mu} &\sqrt{4\pi} \\ &\times \left[\frac{2l+1}{(2\lambda+1)(2l+2\lambda+1)}\right]^{1/2} \\ &\times \left[\frac{(l+\lambda-m+\mu)!(l+\lambda+m-\mu)!}{(l-m)!(l+m)!(\lambda-\mu)!(\lambda+\mu)!}\right]^{1/2} . \end{aligned} \tag{11}$$

These equations are generalizations of the addition theorem[10] of spherical harmonics. The correctness of Eqs. (6), (7), (10), and (11) was tested numerically using Ref. 20. All of the multipole coupling integrals in Eq. (5) can then be done analytically and a set of equations can be generated that can be solved for the multipole coefficients. The result is

$$\sqrt{4\pi}(V_i+E_0Z_i)\delta_{p,0}\delta_{q,0}+\sqrt{4\pi/3}E_0\delta_{p,1}\delta_{q,0} = A(i,p,q)+\sum_{j\ (\neq i),l,m} A(j,l,m)D(p,q,l,m) \times Y_{l+p,m-q}(\theta_{ij},\phi_{ij})\left[\frac{a}{R_{ij}}\right]^{l+p+1}, \quad (12)$$

where θ_{ij} and ϕ_{ij} denote the polar and azimuthal angles from sphere i to sphere j, and R_{ij} is the distance between the centers of the two spheres. We have specialized to the case where all the spheres have the same radius a. This set of equations with $i=1,2,\ldots,N_s$ and p and q running over the $(l_{\max}+1)^2$ multipole terms allows the determination of the multipole coefficients. When the spheres are electrically isolated from one another prior to the first breakdown, constraints are added so that the monopole coefficient on each sphere vanishes. After breakdowns have occurred, the constraints on the monopole coefficients are that the sum of the charges on the spheres in a connected cluster must vanish, and the voltages on all spheres in a cluster is the same. The Appendix gives an example on the use of the method for the case of two spheres in a uniform applied field that is parallel to the line between the centers.

This set of equations has several very nice properties that make the solution quite well behaved numerically. First, the multipole coupling terms fall off in magnitude with powers of the interparticle separation distance, and, in particular, the coupling of higher order multipoles to each other fall off with large powers of this distance. This means that a large number of terms in the matrix are extremely small and can be ignored with negligible impact on the solution. In many cases, the matrix can be made more than 90% sparse, with the solution for the particle voltages in error by less than a few percent. This enables use of sparse-matrix iterative techniques for solving the equations. Second, the use of this coupled multipole expansion technique results in a matrix that is highly diagonal dominated, which means that iterative methods such as the conjugate-gradient algorithm converge very rapidly. In the case of the initial configuration before any local breakdowns occur, the solution usually converges in less than 100 iterations. This, coupled with sparse-matrix-multiplication techniques, results in a very fast numerical solution for the coefficients. Also, since the matrix is sparse, much larger systems of particles can be analyzed with this method than with the boundary element method.[9] The key to the success of this technique, particularly for large systems, is that the neglect of terms in the coupling matrix ignores only the least physically important couplings.

Next we describe how we incorporate breakdown dynamics into this model. The first step is still to identify regions of the sample that are vulnerable to breakdown due to the presence of large electric fields. As in Ref. 9, we continue to approximate the electric field between a pair of particles by the voltage difference between the two conductors divided by their minimum surface-to-surface separation distance d. The voltages can be found straightforwardly from the multipole solution. We still assume that breakdown occurs only between the pair of conductors that has the largest electric field between them as defined above, and define a local breakdown as the formation of an electrical connection between the two conductors. The connection is treated as a thin metallic wire between the conductors that stores negligible charge, so that the net result computationally is to add constraints into the system of equations that provide for the sharing of charge between particles that have been connected and equating their voltages. With these constraints in place, the system of equations is resolved to determine a new set of multiple coefficients and voltages. Using the same criterion for breakdown, we continue this sequence of local breakdowns, storing the field enhancement that caused the local breakdown at each configuration. Here is where some differences begin to appear between the capacitor-plate model and this uniform-field model. We will assume that the sample is broken down completely when a path that is at least one sample radius in length is formed. This rather arbitrary cutoff is made because there is no natural point at which to stop the breakdown process as there was in the capacitor-plate model. A further modification must be made to minimize the effects of fringing fields. Only particles whose distance from the center of the sample is less than 0.8 of the sample radius will be allowed to participate in a local breakdown. This eliminates breakdowns to particles that are at the sample edges and are under the influence of a field that is distorted by edge effects. In this case, edge effects are due to the lack of neighboring particles that would be present in an infinite system. Allowing breakdowns to occur only well within the sample boundaries makes the model one that approximates the breakdown process inside an infinitely large sample, far from any sources or edge effects. The uniform-field description adds another complication in the definition of the breakdown field. The problem is that the average field inside the system is different from the applied field across the sample due to the polarization of the sample. Treating the system for a moment as a uniform dielectric with an effective dielectric constant, it is easy to show that the field inside the dielectric is lower than the applied field. The physical reason for this is that the net dipole moment expels a portion of the applied field. Consequently, any point inside the systems sees an effective applied field that is lower than the actual applied field. This same effect is present in a disordered sample. Thus, all field enhancements calculated in the random samples must be scaled by this effective applied field to create a situation where the applied field across the sample is approximately unity. Furthermore, this effective field changes as breakdowns occur and the sample and the effective dielectric constant increases. This does not create a problem, however; it just means that the field

enhancements at each new configuration must be scaled by the appropriate effective field. Now the minimum field enhancement in this sequence of scaled field enhancements determines the breakdown field of the sample. Hence we define the breakdown field E_b as the inverse of this minimum field enhancement. As such, it is a dimensionless field that is normalized with respect to the breakdown field of the background dielectric.

Finally, we want to define an effective dielectric constant for our samples and look for the behavior of the dielectric constant ϵ as a function of area fraction ϕ. The effective dielectric constant for a medium can be defined as the dielectric constant that an isotropic, homogeneous sample of the same size and shape would need to have in order for it to have the same polarization as the original inhomogeneous sample. For these cylindrical and spherical samples, there is an analytical solution that relates the polarization to the effective dielectric constant;[10] this is one reason why these boundaries were chosen. The polarization is simply the net dipole moment of the random samples, which comes directly out of the multipole solution; it is just the sum of the individual dipole moments on each particle. After breakdowns have occurred, the total dipole moment must include the dipole moments due to charge separation; this is similarly easy to account for, since the monopole terms are also known.

III. MODEL RESULTS

We now turn to a discussion of some results of this model, beginning with a few comments on some of the computational aspects. Samples containing 85 cylindrical inclusions were generated as described in the previous section with area fractions ranging from 0.20 to 0.70 in increments of 0.10. The area fraction 0.70 is just above the freezing transition point in the Monte Carlo hard-disk model,[18] which implies that for area fractions greater than or equal to 0.70, the equilibrium configurations for the cylinders are highly ordered. Hence our configurations at $\phi=0.70$ consist of fluctuations about this equilibrium solid phase configuration which is approximately a triangular lattice. In the 3D model, samples containing 55 spheres were generated with volume fractions ranging from 0.20 to 0.40 in increments of 0.05. A transition to a regular close-packed lattice occurs in the Monte Carlo hard-sphere model at volume fractions just below 0.50. By comparison with exact results for two cylinders in a uniform external field, we found the electric field predicted by using an eighth-order expansion (16 unknowns per cylinder) to be within 1% of the exact result for a surface-to-surface separation distance d of $0.10a$ when neglecting all terms in the matrix with magnitudes less than 10^{-3}. For a surface separation distance $d=0.02a$, the closest allowed spacing, the result was within 10% of the exact result. This represents nearly an order-of-magnitude increase in accuracy over the boundary element method. In three dimensions, the electric field was within 2% of the exact result using a fourth-order expansion (24 unknowns per sphere) and the same matrix cutoff for a separation distance of $d=0.10a$. For the closest spacing $d=0.02a$, the result was also within 12%, indicating that the solution is highly accurate for the sphere problem as well. See the Appendix for more details. Using the eighth-order expansion in two dimensions and fourth-order ($l_{\max}=4$) expansions in three dimensions and neglecting terms in the matrix less than 10^{-3}, the breakdown simulation for 85 cylinders or 55 spheres generates around 300 000 nonzero terms in the matrix at high densities. Solving a system of this size is quite easy from a computational standpoint; a modest workstation can run these simulations in a few h. The results we will describe are insensitive to the number of particles used.

Figure 1 shows equipotential lines for a typical 2D sample at an area fraction $\phi=0.40$ as a demonstration of the multipole expansion solution. The dipole moment of the sample enables us to calculate of the effective dielectric constant and the effective applied field. Figure 2 shows the same sample from Fig. 1 after complete failure, as defined in the previous section. The lines between the particles indicate that a breakdown has occurred between those particles. Note the existence of connections between particles that are not part of the eventual breakdown path. Figure 3 indicates the value of the scaled field enhancement that caused the breakdown of each pair in the sequence. Note that, just as in the capacitor-plate model, the field enhancement does not increase monotonically, and consequently the value of $E_{\max}$ responsible for determining the overall breakdown field (the minimum $E_{\max}$) is not the initial $E_{\max}$ in the virgin sample. The initial $E_{\max}$ does not even scale with the minimum $E_{\max}$ in a simple way, since the initial breakdown is often not on the final breakdown path. Figures 4(a) and 4(b) show plots of the breakdown field E_b as a function of area fraction ϕ for the 2D model and volume fraction ϕ for the 3D model. Ten samples were generated at each area and volume fraction, and the breakdown simulations were run until the global breakdown criterion was met. The results were averaged over these ten runs and the error bars on the plots in the figure represent one

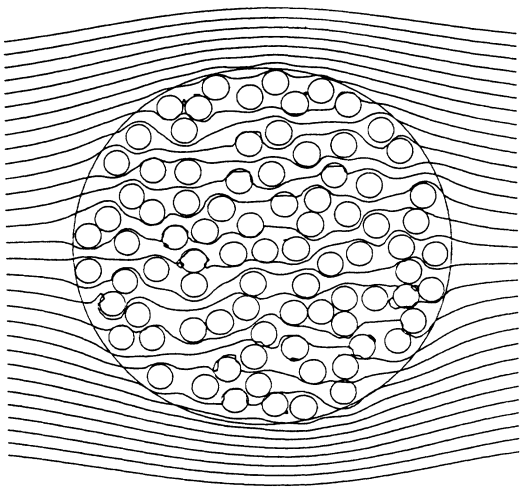

FIG. 1. Equipotentials for a typical 2D sample with an area fraction $\phi=0.40$.

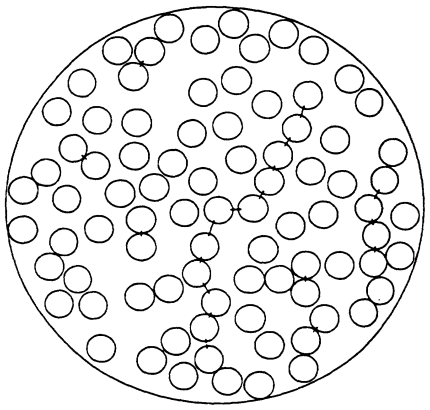

FIG. 2. Final breakdown path illustrated for the sample in Fig. 1.

standard deviation about those averages. The breakdown field decreases monotonically with increasing area fraction, as expected, and E_b approaches a small but finite value as the random close-packing limit ϕ_c is approached. Note that the breakdown field cannot go to zero because the oxide layers prevent contact between the cylinders. These results are totally consistent with the results obtained in the capacitor-plate model.

Figures 5(a) and 5(b) display plots of the effective dielectric constant ϵ as a function of ϕ for both the 2D and 3D models. The dielectric constant increases monotonically with increasing area and volume fraction; this is easily explained physically by noting that the polarization

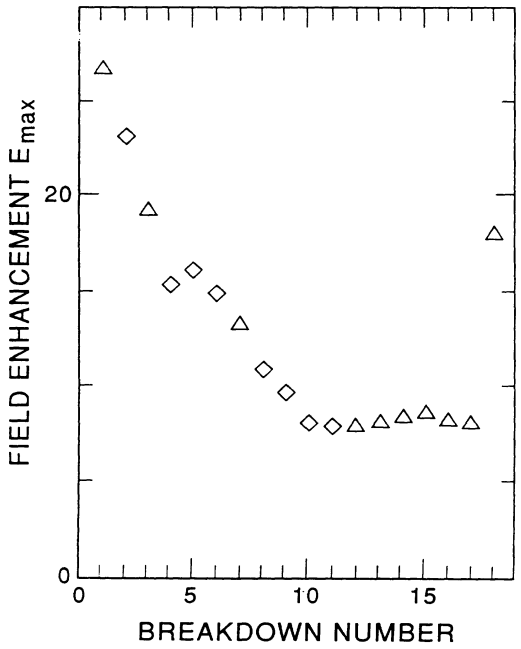

FIG. 3. Evolution of the maximum field enhancement E_{max} for the breakdown sequence shown in Fig. 2. The triangles represent connections that were on the final breakdown path and the diamonds represent isolated connections.

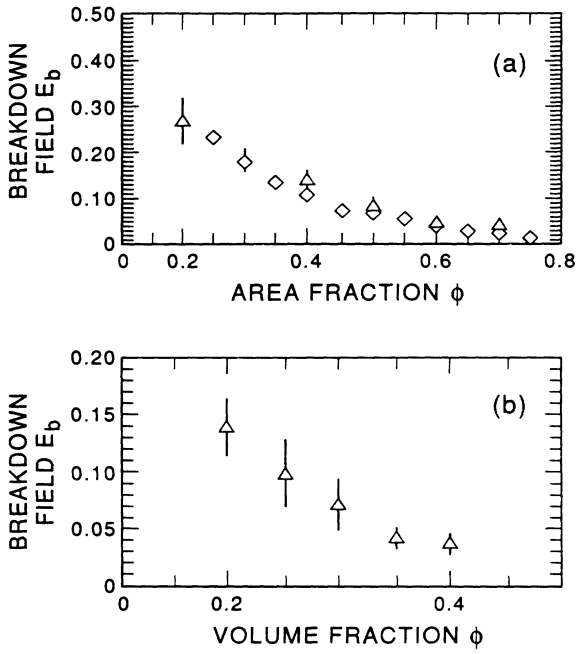

FIG. 4. (a) Average breakdown field E_b for the 2D random cylinder arrays. (b) Average breakdown field E_b for the 3D random sphere arrays.

of each sample clearly increases with increasing metal fraction. In addition, ϵ diverges as $\phi \rightarrow \phi_c$. This effect was seen in the capacitor-plate model and has been measured experimentally in systems of silver particles randomly embedded in a KCl matrix[21] and in a system of metal spheres in wax.[22] Figure 5 also shows two analyti-

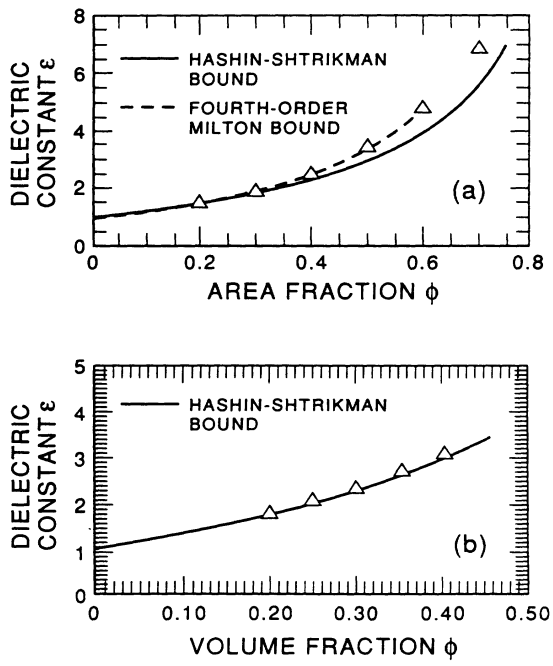

FIG. 5. (a) Average effective dielectric constant ϵ for the 2D random cylinder arrays. (b) Average effective dielectric constant ϵ for the 3D random sphere arrays.

cally derived lower bounds that can be placed on ϵ for any isotropic two-phase materials;[23] no upper bound exists if one phase is perfectly conducting. The Hashin bound is the best possible lower bound for a statistically isotropic two-phase material given only volume or area fraction information. The fourth-order Milton bound[23] includes information on the statistical distribution of phases and thus is a tighter bound, but it contains some approximations that start to break down as $\phi \rightarrow \phi_c$. Our data as shown in Figure 5 are consistent with the bounds described above. Another numerical method that is useful for determining the dielectric constant of a random array of conducting particles is described by Torquato and Kim and by Tobochnik, Laing, and Wilson.[24]

IV. SCALING OF THE BREAKDOWN FIELD

Earlier we indicated the desire to confirm the scaling results found in the capacitor plate model for larger 2D systems and for 3D systems using this uniform-field description. The first scaling relation we will check is the minimum gap. The actual minimum gap for these samples is undefinable for the uniform-field model, since there is no fixed starting point or ending point for the breakdown path. However, it is possible to define a normalized dielectric gap as the length of the breakdown path through the dielectric divided by the vertical distance traversed by the entire path. Hence, although no two paths are the same length, they can be normalized in a consistent way. The question of whether or not these paths correspond to minimum gap paths is one that simply cannot be answered with this model. However, the scaling of the breakdown field with the average normalized dielectric gap as defined above can still be investigated. The gap decreases monotonically as the area fraction increases, and the results are similar to those obtained using the capacitor-plate model. The 2D and 3D results are qualitatively similar. Figure 6(a) shows a plot of the breakdown field E_b as a function of the average normalized dielectric gap $\bar{x}$ for the 2D uniform-field model. Note that the breakdown field scales linearly with $\bar{x}$ over the entire range of data. This is entirely expected based on the results of the capacitor-plate model. In three dimensions we expect the same result to hold; the argument given in Ref. 9 for the scaling of E_b with the minimum gap is equally valid in three dimensions. Figure 6(b) shows a plot of the breakdown field E_b as a function of the average normalized dielectric gap for the 3D model. The breakdown field again scales linearly with $\bar{x}$ and is consistent with the 2D results.

Next we will consider the scaling of the breakdown field with the average surface-to-surface separation distance of nearest-neighbor cylinders $\bar{d}$, which we normalize with respect to the cylinder radius a. As with $\bar{x}$, $\bar{d}$ decreases monotonically as ϕ increases. Furthermore $\bar{d} \rightarrow 0.02a$ as $\phi \rightarrow \phi_c$ due to the presence of the oxide layer. For a closely spaced regular lattice of particles, it is easy to show that the field between the particles is given by $E = E_{\text{applied}}(D+d)/d$ for the applied field along the closest-packed direction, where $D = 2a$ is the sphere diameter. Therefore, one would expect that the breakdown

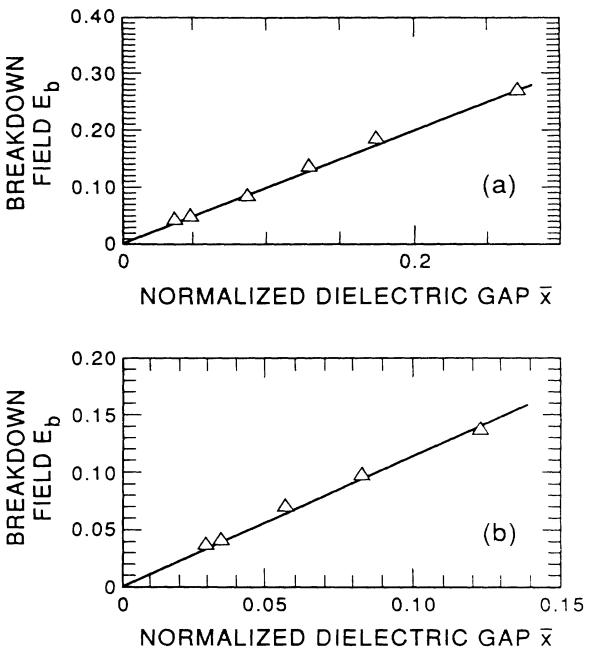

FIG. 6. (a) Scaling of the breakdown field with the average normalized dielectric gap for the 2D model. (b) Same data for the 3D model.

field would scale linearly with the parameter $\bar{d}/(D+\bar{d})$ in a random system, i.e.,

$$E_b = E_b^{\text{binder}} \frac{\bar{d}}{D+\bar{d}} . \tag{13}$$

Figure 7 shows a plot of E_b as a function of reduced sepa-

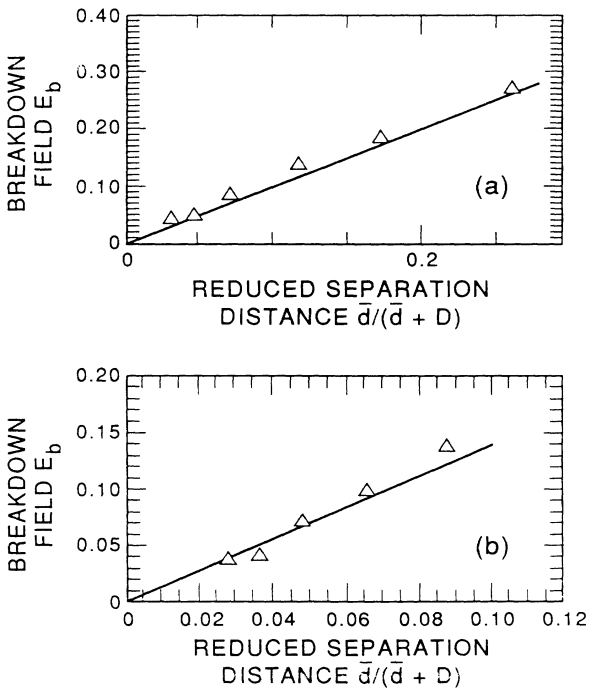

FIG. 7. (a) Scaling of the breakdown field with the reduced nearest-neighbor separation distance for the 2D model. (b) Same data for the 3D model.

ration distance $\bar{d}/(D+\bar{d})$ for both the 2D and 3D models. Notice that E_b does indeed scale linearly with this reduced separation distance. In the next section, it will be shown that the average nearest-neighbor separation distance can be determined for real materials using ideas from the theory of simple liquids.[25] This will enable us to make a connection between this theory and actual experimental data on the breakdown field.

V. COMPARISON TO EXPERIMENTAL RESULTS

In the previous section, it was demonstrated that the breakdown field can be calculated in a random array of up to 100 or more particles. As was shown, the breakdown field scales in a simple fashion with the average surface-to-surface distance between nearest-neighbor metal particles in the composite, i.e., $E_b \approx E_b^{\text{binder}} \bar{d}/(D+\bar{d})$. This connection between breakdown field and metal nearest-neighbor spacings can be exploited to make predictions of the breakdown field in complicated composites. In order to test the theory, we made comparisons with a set of dielectric breakdown measurements made by Covino and Hudson[26] on a series of inert propellant samples. The samples consisted of 3-μm diam aluminum particles and large (200–550-μm) sodium chloride particles in a hydroxyl-terminated polybutadiene binder. The mix parameters are listed in Table I.

We chose these data since the samples were well characterized by several techniques and a large number of breakdown tests were applied to each sample type. This was possible since the samples were inert (the oxygen-supplying ammonium perchlorate had been replaced by sodium chloride). Some theoretical method was needed to determine the average nearest-neighbor distances in this composite. Rather than using Monte Carlo methods, which can be difficult at large volume fractions and in cases where the particle sizes vary over several orders of magnitude, we chose to use correlation function techniques developed to deal with the statistical mechanics of simple liquids. The microgeometry is determined by appealing to the Boltzmann hypothesis in statistical mechanics; i.e., in a well-stirred sample, all configurations with the same energy have the same *a priori* probability. We chose to model the particles in the composite as hard spherical particles that cannot overlap; otherwise, any configuration is possible and all configurations have the same energy.

The microgeometry of the sample is well characterized by the pair-correlation function[25] $g(r)$, which describes the relative probability of finding the centers of two particles a specified distance from each other in the composite. From this function one can determine the nearest-neighbor distribution function and the average surface-to-surface distance between metallic particles in the composite. This can then be used with Eq. (13) to predict the breakdown field of the sample. If one knows the pair-correlation function of a material, then the nearest-neighbor-distance distribution function is given by

$$p(r)=4\pi n\, g(r) r^2 \exp\left[-4\pi n \int_0^r g(r') r'^2 dr'\right], \quad (14)$$

where $p(r)dr$ is the probability that the nearest neighbor of a given particle is between r and $r+dr$, and n is the number density of particles. This is easily proven, since $4\pi n g(r) r^2 dr$ is the average number of particles in a shell of thickness dr at a distance r from a chosen particle. The probability that there are no particles closer than r to a given particle is given by

$$P(r)=\prod_{k=1}^{r/\Delta r}[1-4\pi n\, g(k\Delta r)(k\Delta r)^2 \Delta r] .$$

The shell width Δr is chosen so that $4\pi n\, g(k\Delta r)(k\Delta r)^2 \Delta r \ll 1$ for all k. Taking the logarithm of both sides, converting the sum into an integral by taking the limit of $\Delta r \to 0$, and noting that $p(r)=dP/dr$ we get Eq. (14). The average surface-to-surface distance between spheres is

$$\bar{d}=\int_0^\infty p(r) r\, dr - D , \quad (15)$$

where D is the diameter of a sphere.

The pair-correlation functions of a composite are determined from the number densities of the components of the mixture as long as the sample is well stirred and hence obeys the Boltzmann conjecture. There exist a number of approximation schemes in statistical mechanics for determining the pair-correlation function. One method that works well for hard-sphere potentials is the

TABLE I. The mix parameters in the samples used by Covino and Hudson (Ref. 25). The breakdown field was obtained at 17°F and at 14% relative humidity. The final column is the theoretically determined average nearest-neighbor surface-to-surface distance between metal particles divided by the metal particle diameter. These values are determined from Eqs. (14) and (15) using the pair correlation function for hard spheres as determined from the Percus-Yevick approximation.

Sample	Volume (%) 3 μm Al	NaCl	Experimental breakdown field (MV/m)	$\bar{d}/D$
1	12.7	47.5	1.65	0.087
2	22.4	35.9	0.75	0.045
3	33.4	25.0	0.45	0.025
4	3.0	55.7	4.7	0.327
5	54.7	0.0	0.25	0.013

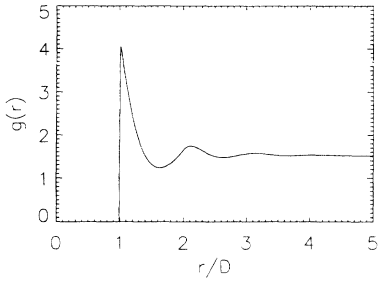

FIG. 8. The pair-correlation function $g(r)$ for metal particles in sample number 2 in Table I.

Percus-Yevick (PY) approximation.[25,27–29] This method is well tested and remains quite accurate even at high densities near the phase transition to a solid structure.[25] In addition, it has the added advantage that the pair-correlation functions can be determined analytically for hard spheres even for the case where two different sphere sizes are present.[29] Figure 8 displays the pair-correlation function for the metallic particles for composite number 2 in Table I using the specified particle sizes and amounts. The large salt particles were assumed to all have a diameter of 300 μm and the aluminum particles were all assumed to have diameters of 3 μm. Distance in the figure is measured in units of the aluminum particle diameter. The pair-correlation function does eventually tend to unity at large distances on a scale set by the large-particle size. One might note that the PY approximation leads to the pair-correlation function between the large particles being negative for these densities and particle size ratios. We have not used the large-particle correlation function for the calculation of the distance between metal particle nearest neighbors. As a check of the validity of the scheme, we also calculated the nearest-neighbor distances using the one sphere size solution of the Percus-Yevick equation and assumed that the large salt particles only contributed to an excluded-volume effect for the small aluminum particles. This is a good approximation in this case due to the large ratio of sizes of the particles. The results are essentially identical. The nearest-neighbor-distance distribution function between metal particles is determined from $g(r)$ using Eqs. (14) and (15) and is shown in Fig. 9. The values determined from these calculations are listed in Table I.

Now we can test Eq. (13) to see if it gives an accurate

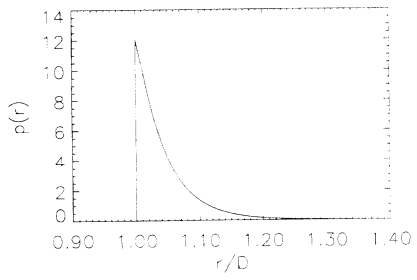

FIG. 9. The nearest-neighbor-distance distribution function for sample number 2 in Table I.

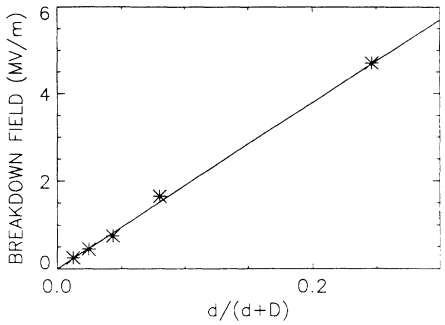

FIG. 10. The experimental breakdown field of the samples in Table I vs the theoretically determined value for $\bar{d}/(D+\bar{d})$. The slope of the line is 19 MV/m, in good agreement with the experimental value of 23 MV/m (Ref. 26).

representation of the breakdown field in these propellants. Figure 10 displays the experimentally determined breakdown field[26] plotted as a function of the theoretically determined scaled nearest-neighbor distance $\bar{d}/(D+\bar{d})$. Note that all five samples fall onto the same straight line, as predicted. Furthermore, from Eq. (13) the slope of that line should be the breakdown field of the binder. The slope of the line is 19 MV/m, in good agreement with the experimental value of 23 MV/m.[26] Note from Table I that the breakdown field of sample number 5 is about one hundredth of the value of the pure binder, and so the addition of metal particles to the composite can have a huge effect on the breakdown field. This method also gives good agreement with the experimental dielectric breakdown results obtained for metallic spheres embedded in wax.[22]

These results confirm that the breakdown field in metal-loaded dielectrics scales in a simple fashion with the average distance between metallic particles even in complex composites, and that the cause of the low breakdown fields in these materials is the field enhancement due to the metal particles in the composite. Hence, we can use this simple scaling to predict the breakdown fields in complex composites from knowledge of the microstructure of the composite. Since this problem is much easier than the determination of the electric-field patterns in complex composites, this will allow quick and easy predictions of breakdown strengths of materials simply based upon their mixture parameters. Generalizations of the theory to cases with more than two particle sizes are possible and will be useful for mixtures containing multimodal particle-size distributions.

VI. CONCLUSION

To summarize, we have presented a model for dielectric breakdown in random metal-loaded dielectrics that incorporates continuous geometry effects. It is a more realistic model than lattice models, which have been focused on up to this point, and is capable of handling significantly larger system sizes than the previously introduced capacitor-plate model. In many instances, our results have confirmed results found in previous models,

and in a few cases some insights have been gained. Specifically, our model predicts that the breakdown field E_b goes to zero as the metal fraction ϕ approaches the close-packing limit for this model and the effective dielectric constant ϵ approaches a large but finite value; the dielectric constant cannot diverge due to the finite minimum separation between particles imposed by the presence of the oxide layers. These results are qualitatively in agreement with the aforementioned lattice results and results from the capacitor-plate model. In addition, we have identified two geometrical parameters, the normalized dielectric gap $\bar{x}$ and the average nearest-neighbor separation distance $\bar{d}$, which scale linearly with the breakdown field over the entire range of metal fractions studied. These results should allow for the estimation of the effect of mixture composition in a straightforward way. The theory was applied to a set of experimental data that confirmed the simple scaling relationship between the breakdown field and the metallic particle nearest-neighbor distance in the composite. Further details of this work and the work in Ref. 9 can be found in Ref. 30.

ACKNOWLEDGMENTS

The authors wish to thank U.S. Army Research Office (Contract No. DAAL03-87-C-0021, Project Number P-24927-EG-S) for supporting this work. In addition, we would like to thank Ron Larson and Jim Lindsay of Electromagnetic Applications Inc. for their many suggestions.

APPENDIX

We will give an example of how to use Eq. (12). We will determine the voltage of a pair of conducting spheres of radius a in a uniform applied electric field E_0, which is parallel to the line between the centers of the spheres. We take this direction to be the z axis and the centers of the spheres to be located at $\pm z_0$. We can determine the accuracy of the solution by comparing the calculated voltages with the exact solution[31]

$$V_0 = \mp E_0 a \sinh(\eta_0) \frac{\sum_{n=0}^{\infty} [(2n+1)/(e^{(2n+1)\eta_0}-1)]}{\sum_{n=0}^{\infty} [1/(e^{(2n+1)\eta_0}-1)]} \quad \text{(A1)}$$

where

$$\eta_0 = \ln\left[\frac{(d^2+2ad)^{1/2}+d}{(d^2+2ad)^{1/2}-d}\right]$$

and $d = z_0 - a$ is *one-half* of the surface-to-surface distance between the spheres.

The method of solving Eq. (12) is to solve the linear set of equations

$$Bx = b \ , \quad \text{(A2)}$$

where the unknown vector x is the multipole coefficients $A(i,l,m)$ and the voltages V_i. Due to the symmetry, only the $m=0$ terms contribute in this case, so there are $N_s(l_{\max}+1)+N_s$ unknowns ($N_s=2$ here):

$$x_k = \begin{cases} A(i,l,0) & \text{for } k=(i-1)(l_{\max}+1)+l+1 \\ V_i & \text{for } k=N_s(l_{\max}+1)+i \ , \end{cases}$$

where $i=1,2$ and $l=0,1,\ldots,l_{\max}$. The right-hand side of equation (A2) contains the applied field contributions of equation (12):

$$b_k = \begin{cases} E_0 a\sqrt{4\pi/3} & \text{for } k=2 \text{ and for } l_{\max}+3 \\ E_0 z_0 \sqrt{4\pi} & \text{for } k=1 \\ -E_0 z_0 \sqrt{4\pi} & \text{for } k=l_{\max}+2 \\ 0 & \text{otherwise} \ . \end{cases}$$

Finally, the matrix elements of the matrix B are given by the following: (a) for $i=j$, $B_{kq}=1$ if $p=l$ and $B_{kq}=0$ if $p\neq l$; (b) for $i\neq j$, $B_{kq} = D(p,0,l,0)Y_{l+p,0}(\theta_{ij},\phi_{ij})(a/R_{ij})^{l+p+1}$, where $k=(i-1)(l_{\max}+1)+l+1$ and $q=(j-1)(l_{\max}+1)+p+1$.

The constraint column, which couples the sphere voltages to the applied field, is $B_{kq}=-\sqrt{4\pi}$ for $k=1$, $q=N_s(l_{\max}+1)+1$ and for $k=l_{\max}+2$, $q=N_s(l_{\max}+1)+2$. Finally, the constraint row, which insures that the net charge on each sphere vanishes, is $B_{kq}=1$ for $k=N_s(l_{\max}+1)+1$, $q=1$ and for $k=N_s(l_{\max}+1)+2$, $q=l_{\max}+2$. All other elements in the matrix vanish.

The solution of the linear equations here and in the calculation in the body of the paper is done by standard numerical methods.[32] As evidence of the accuracy of the solution, Table II compares the multipole solution with the exact solution.[31] The electric field and the sphere radius are set to unity.

TABLE II. As can be seen in the table, by keeping multipole terms up to $l_{\max}=4$, we make an error of no more than 11.6% for the worst case of two spheres that are 0.01 diameters apart. For the more typical case of spheres that are 0.1 diameters apart, the error is less than 0.3%. This is the more important case, since, as discussed in the text, it is spheres that are an average distance apart rather than ones that are almost touching that determine the final breakdown strength.

$l_{\max}$	V	Accuracy (%)
	$z_0=1.10$	
1	0.8456	4.8
2	0.8225	2.0
3	0.81275	0.77
4	0.80890	0.29
5	0.80743	0.11
	0.80655	exact
	$z_0=1.01$	
1	0.6864	36.8
2	0.6315	25.8
3	0.5947	18.5
4	0.569 96	11.6
5	0.553 01	8.2
10	0.519 45	3.5
	0.510 845	exact

*Present address: Center for Polymer Studies, Department of Physics, 590 Commonwealth Ave., Boston University, Boston MA 02215.

[1]R. Kent and R. Rat, J. Electrostat. **17**, 299 (1985); Aviat. Week Space Technol. **122** (3), 23 (1985); **122** (17), 44 (1985); **122** (18), 24 (1985).

[2]L. de Arcangelis, S. Redner, and H. J. Herrmann, J. Phys. (Paris) Lett. **46**, L585 (1985); M. Soderberg, Phys. Rev. B **35**, 352 (1986).

[3]P. M. Duxbury, P. D. Beale, and P. L. Leath, Phys. Rev. Lett. **57**, 1052 (1986).

[4]P. D. Beale and P. M. Duxbury, Phys. Rev. B **37**, 2785 (1988).

[5]D. R. Bowman and D. Stroud, Phys. Rev. B **40**, 4641 (1989).

[6]Y. Gefen, W. H. Shih, R. B. Laibowitz, and J. M. Viggiano, Phys. Rev. Lett. **57**, 3097 (1986).

[7]H. Takayusu, Phys. Rev. Lett. **54**, 1099 (1985).

[8]S. S. Manna and B. K. Chakrabarti, Phys. Rev. B **36**, 4078 (1987); R. B. Stinchcombe, P. M. Duxbury, and P. Shukla, J. Phys. A **19**, 3903 (1986); P. M. Duxbury, P. Shukla, R. B. Stinchcombe, and J. M. Yeomans (unpublished); B. K. Chakrabarti, K. K. Bardan, and P. Ray, J. Phys. C **20**, L57 (1987); B. K. Chakrabarti, in *Reviews of Solid State Science* (World Scientific, Singapore, 1990).

[9]M. F. Gyure and P. D. Beale, Phys. Rev. B **40**, 9533 (1989).

[10]J. D. Jackson, *Classical Electrodynamics* (Wiley, New York, 1962).

[11]M. Danos and L. Maximon, J. Math. Phys. **6**, 766 (1965).

[12]B. C. Carlson and G. S. Rushbrooke, Proc. Cambridge Philos. Soc. **46**, 626 (1950).

[13]M. E. Rose, J. Math. Phys. **37**, 215 (1958).

[14]R. A. Sack, J. Math. Phys. **5**, 245 (1964); **5**, 252 (1964); **5**, 260 (1964).

[15]L. Greengard, *The Rapid Solution of Potential Fields in Particle Systems* (MIT, Cambridge, MA, 1987).

[16]K. E. Schmidt and M. A. Lee, J. Stat. Phys. **63**, 1223 (1991).

[17]I. L. Davis, J. Appl. Phys. **67**, 1022 (1990).

[18]I. S. Gradshteyn and I. M. Ryzhik, *Tables of Integrals, Series and Products* (Academic, New York, 1965).

[19]L. D. Landau and E. M. Lifshitz, *Quantum Mechanics* (Pergamon, Oxford, 1977).

[20]S. Wolfram, *Mathematia* (Addison-Wesley, New York, 1988).

[21]D. M. Grannan, D. C. Garland, and D. B. Tanner, Phys. Rev. Lett. **46**, 375 (1981).

[22]P. M. Duxbury, P. D. Beale, and H. Bak, J. Phys. D **23**, 1554 (1989).

[23]Z. Hashin and S. Shtrikman, J. Appl. Phys. **33**, 3125 (1962); S. Torquato and F. Lado, Proc. R. Soc. London, Ser. A **59**, 417 (1988); G. W. Milton, J. Appl. Phys. **52**, 5294 (1981).

[24]S. Torquato and I. C. Kim, Appl. Phys. Lett. **55**, 1847 (1989); J. Tobochnik, Comput. Phys. **4** (2), 181 (1990); J. Tobochnik, D. Laing, and G. Wilson, Phys. Rev. A **41**, 3052 (1990).

[25]J. P. Hansen and I. R. McDonald, *Theory of Simple Liquids* (Academic, London, 1986).

[26]J. Covino and F. Hudson, J. Propulsion and Power (to be published); private communication.

[27]J. K. Perkus and G. J. Yevick, Phys. Rev. **110**, 1 (1957).

[28]M. S. Wertheim, Phys. Rev. Lett. **10**, 321 (1963); E. Theile, J. Chem. Phys. **39**, 474 (1963).

[29]J. L. Lebowitz, Phys. Rev. **133**, A895 (1964).

[30]M. F. Gyure, Ph.D. thesis, University of Colorado at Boulder, 1990.

[31]M. Hara and M. Ahazahi, J. Electrostat. **2**, 223 (1976–1977).

[32]W. A. Press, B. P. Flannery, S. A. Teukolsky, and W. T. Vetterling, *Numerical Recipes* (Cambridge University, Cambridge, England, 1986).